Chapter

Power Device Loss Analysis of a High-Voltage High-Power Dual Active Bridge DC-DC Converter

Thaiyal Naayagi Ramasamy

Abstract

The insulated-gate bipolar transistor (IGBT) offers low conduction loss and improved performance and, hence, is a potential candidate for high-current and high-voltage power electronic applications. This chapter presents the power loss estimation of IGBTs as employed in a high-voltage high-power dual active bridge (DAB) DC-DC converter. The mathematical models of the device currents are derived, and the power loss prediction is clearly explained using the mathematical models. There are many parameters to consider when selecting an appropriate power device for a given application. This chapter highlights the step-by-step procedure for selecting suitable IGBTs for a 20 kW, 540/125 V, 20 kHz DAB converter designed for aerospace energy storage systems. Experimental results are given to demonstrate the device performance at 540 V, 80 A operation of high-voltage IGBTs and 125 V, 300 A operation of low-voltage IGBTs and thus validate the selection procedure presented.

Keywords: power loss prediction, HV-side IGBTs, LV-side IGBTs, zero voltage switching, zero current switching, dual active bridge, DC-DC converter

1. Introduction

The dual active bridge (DAB) [1, 2] is a bidirectional DC-DC converter that has a small transformer between the two active bridges. This topology has received significant attention from researchers for high-power applications for decades. Compared with a single-phase DAB, a three-phase DAB of similar rating offers the benefits of smaller passive components and improved magnetic utilization [3]. Acronyms used in this chapter are listed in **Table 1**. A high-voltage SiC IGBT is used to achieve optimum design of a DAB converter based on the consideration of the device and transformer characteristics in [4]. However, the high *dv/dt* of the SiC IGBT switches [5–7] causes a huge spike and ringing in the currents during hard switching at high voltage levels.

An optimization algorithm for non-active power loss minimization in the DAB DC-DC converter is discussed in [8] to improve the converter efficiency. Ref. [9] presents an advanced control strategy to reduce DAB converter losses. A survey of material-level developments in the key components of PWM power converters and the potential for improving system power density using advanced components is presented in [10]. Ref. [11, 12] indicate that a reduction of the switching loss by tenfold

Acronyms	Abbreviations
SiC	Silicon carbide
PWM	Pulse width modulation
HV	High voltage
LV	Low voltage
DAB	Dual active bridge
IGBT	Insulated-gate bipolar transistor
MOSFET	Metal-oxide-semiconductor field-effect transistor
DC	Direct current
ZVS	Zero voltage switching
ESR	Effective series resistance
ZCS	Zero current switching

Table 1.
List of acronyms and their abbreviations.

is achievable with the use of such advanced devices. Although wide bandgap devices have merits over Si devices, most have not been commercialized due to various reasons, such as the difficulty of mass producing large-diameter SiC wafers, the difficulty of controlling the impurity level of these devices, and high cost. Several parameters must be considered to select the correct power semiconductor device for any power electronic circuit. Device output characteristics, thermal characteristics, switching characteristics, blocking voltage, leakage current, and safe operating area (SOA) are all important factors with respect to reliability. It is important to note that at any point of time during device operation, the maximum ratings specified in the device datasheet should not be exceeded [13–15]. The gate charge characteristics and gate driver requirements of a power device and the associated driver circuit loss are also important factors to be considered when selecting an appropriate power device. The focus of this chapter is the estimation of the conduction power loss and the switching power loss. The key parameters and the device characteristics portrayed in the datasheets are discussed in [16].

The DAB DC-DC converter is shown in **Figure 1**. The converter has two H-bridge circuits interfaced via a high-frequency transformer. To correctly choose

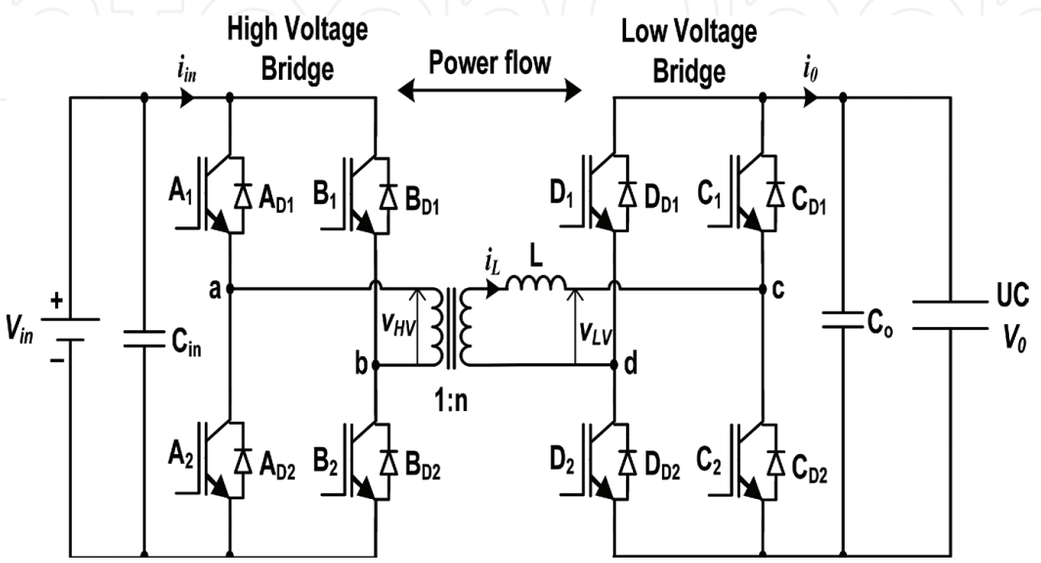

Figure 1.
Dual active bridge DC-DC converter.

the power device for the DAB, power loss calculation is performed for all power devices under the worst-case operating condition of the converter.

The performances of various metal-oxide-semiconductor field-effect transistors (MOSFETs) and IGBTs produced by commercial manufacturers are compared to determine the appropriate power semiconductor device for the high-voltage (HV) and low-voltage (LV) sides of the converter [17–21]. For mission-critical applications such as aerospace systems, voltage transients are inevitable and are taken into consideration when selecting the voltage ratings of devices: 1200 V IGBTs are chosen for the HV side, and 600 V IGBTs are chosen for the LV side [22]. In addition to the device voltage and current handling capabilities and the power density, the anti-parallel diode's on-state voltage and soft recovery characteristics should be taken into consideration. An analysis of MOSFET usage for the low-voltage side of the converter is presented in [23]. Due to the low voltage on the secondary side, the devices should be able to handle high currents. Hence, three or more MOSFETs should be connected in parallel, which makes the circuit very complex. Consequently, IGBT technology [24–26] has been chosen due to its high-current and high-voltage handling capabilities. The IGBT power modules have the benefit of reduced internal inductance and improved heat dissipation and are easy to connect. This chapter discusses the selection procedure of appropriate power devices for a high-power DAB DC-DC converter design. The mathematical model of the device current equations is presented. Researchers at an early stage of their research will find this information valuable as a reference for the design and development of converter prototypes.

This chapter significantly extends the experimental results given in [16]. Specifically, the experimental results for high-voltage IGBTs with the snubber capacitor and for low-voltage IGBTs with and without the snubber capacitors are included. In addition, the experimental measurements of power losses of the HV- and LV-side IGBTs are presented. The remainder of this chapter is organized as follows. The power loss estimation of HV- IGBTs of the converter from various manufacturers is presented in Section 2. Section 3 discusses the power loss calculation of LV-side IGBTs and the loss comparison of IGBTs with similar ratings from various leading manufacturers. The experimental results are presented in Section 4, and the conclusions are given in Section 5.

2. Power loss estimation of HV-side devices of the DAB DC-DC converter

To select the correct device, a power loss calculation should be performed for the worst-case scenario of the converter for the chosen application. In this work, we consider the design of a DAB converter for an aerospace energy storage system whose HV side is connected to the DC link of an aircraft and its LV side is connected to an ultracapacitor-based energy storage system. The working range for the ultracapacitor is assumed to be 2:1. The worst-case operating condition of the converter is V_{HV} = 540 V, V_{LV} = 62.5 V, inductor RMS current I_{RMS} = 427 A, peak inductor current I_P = 640 A, average ultracapacitor current I_0 = 320 A, power throughput P_0 = 20 kW, and d = 0.5. The main component values of the converter are determined by applying the worst-case operating condition to the equations derived based on the mathematical model of the DAB converter, which are presented in [16, 27].

The loss calculation is performed for the devices provided by various leading manufacturers for a 20 kHz switching frequency. The theoretical waveforms of the converter and the device currents are illustrated in **Figure 2**. The terms and symbols used in the analysis are listed in **Table 2**. Piecewise linearity is assumed for the

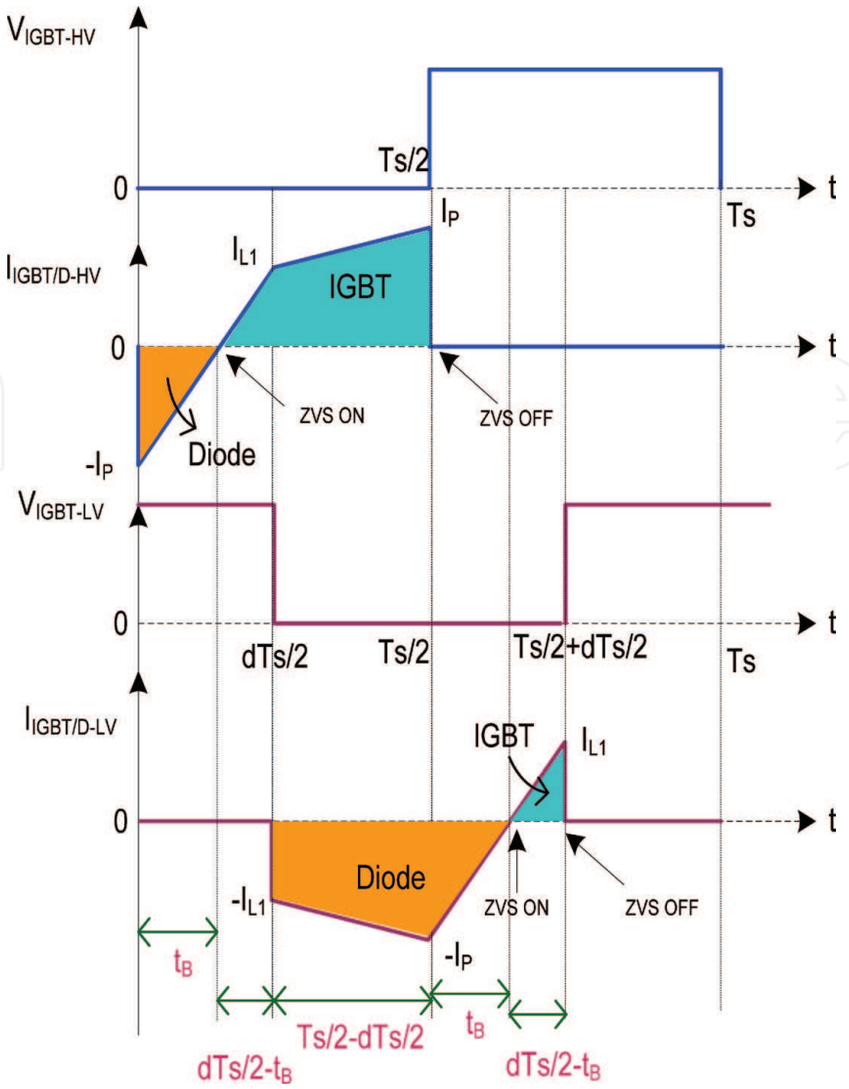

Figure 2.
Theoretical waveforms of devices on the HV side and LV side of the DAB DC-DC converter. (Device conduction intervals are marked in pink).

device current waveforms. Hence, the average current flow through the IGBT on the HV side of the converter during the on-time is given by

$$I_T = \frac{\frac{1}{2} \times I_{L1} \times \left(\frac{dT_S}{2} - t_B\right) + \frac{1}{2} \times (I_{L1} + I_P) \times \left(\frac{T_S}{2} - \frac{dT_S}{2}\right)}{\frac{T_S}{2} - t_B} \quad (1)$$

The IGBT has a constant voltage drop during the on-state. Hence, the conduction loss can be calculated using the average IGBT current and the duty cycle, which is given as

$$P_{CondT} = V_{CE(sat)} \times I_T \times d \quad (2)$$

The duty cycle is the ratio of the on-period of the transistor to the switching period. The datasheet specifies the forward voltage drop of the transistor ($V_{CE(sat)}$) and the anti-parallel diode (V_F) with respect to the main terminals of the modules, which includes the voltage drops across the terminals. Due to the high power densities of the devices, terminal losses cannot be neglected compared with the semiconductor losses. Hence, it is important to specify the voltage drop at the chip level and across the terminals (r_{CE}') separately. The voltage drop across the terminals is given by

$$V_{CE(sat)} = V_{CEO} + (r_{CE} \times I_T) \quad (3)$$

The average diode current on the HV side of the converter during the on-state, as shown in **Figure 2**, is given as

$$I_D = \frac{1}{2} \times I_P \quad (4)$$

In Eq. (4), the diode conduction interval and the base interval are the same on the HV side; hence, the diode current is computed regardless of time. Assuming a constant voltage drop, the conduction losses of the diode are estimated as

Symbols/terms	Description
d	Duty cycle
T_s	Switching time period
I_T	Transistor current
I_P	Peak inductor current
I_{L1}	First inductor current peak
t_B	Time interval from I_P to zero current
$V_{CE\ (sat)}$	Transistor forward voltage drop
P_{CondT}	Transistor conduction loss
r_{CE}	Collector to emitter resistance
V_{CEO}	Collector to emitter voltage with gate open
I_D	Diode current
P_{CondD}	Diode conduction loss
V_F	Diode forward voltage drop
P_C	Total conduction loss
P_{ON}	Transistor turn-on power loss
E_{ON}	Transistor turn-on energy loss
f	Switching frequency
P_{OFF}	Transistor turn-off power loss
E_{OFF}	Transistor turn-off energy loss
V_{CE}	Collector to emitter voltage
I_C	Collector current
t_r	Rise-time
t_f	Fall-time
P_{SW}	Total switching loss
$R_{th(c-s)}$	Case to sink thermal resistance
$R_{th(j-c)}$	Junction to case thermal resistance
P_T	Total power loss
T_{jIGBT}	Junction temperature of IGBT
T_{jDiode}	Junction temperature of diode

Table 2.
List of symbols/terms used in analysis and their description.

$$P_{CondD} = V_F \times I_D \times d \tag{5}$$

The DAB converter has four transistors and four antiparallel diodes on the HV side. Hence, the total conduction loss P_C of the semiconductor devices on the HV side of the converter is given as

$$P_C = 4 \times (P_{CondT} + P_{CondD}) \tag{6}$$

Switching losses are calculated from the turn-on (E_{ON}) and turn-off (E_{OFF}) energy loss curves, which are usually given as a function of the collector current at the switching instants of an IGBT, as given in the manufacturer datasheet. In the DAB converter configuration under zero voltage switching (ZVS), the diode always turns off with zero current, thus eliminating the diode reverse recovery losses. Therefore, the power loss equations for the turn-on and turn-off instants are

$$P_{ON} = E_{ON} \times f \tag{7}$$

and

$$P_{OFF} = E_{OFF} \times f \tag{8}$$

P_{ON} is the power loss during the turn-on instant, P_{OFF} is the power loss during the turn-off instant, and f is the switching frequency. In some manufacturers' datasheets, the energy loss curves for turn-on and turn-off may not be available. For those cases, it is necessary to consider the simplified voltage and current waveforms during the switching process. Switching losses are predominant during the rise-time and fall-time periods. Hence, the loss equations are approximated during the turn-on and turn-off instants, which are given as

$$P_{ON} = \frac{1}{2} V_{CE} \times I_C \times t_r \times f \tag{9}$$

and

$$P_{OFF} = \frac{1}{2} V_{CE} \times I_C \times t_f \times f \tag{10}$$

In DAB converter operation during ZVS, the anti-parallel diode current is always transferred to the IGBTs. Hence, the turn-on switching losses can be neglected. Therefore, the total switching losses (P_{SW}) are approximated as

$$P_{SW} = 4 \times [E_{OFF} \times f] \tag{11}$$

The junction temperature of the devices is calculated as

$$T_{jIGBT} = T_s + (P_T \times R_{th(c-s)}) + (P_{IGBT} \times R_{th(j-c)}) \tag{12}$$

and

$$T_{jDiode} = T_s + (P_T \times R_{th(c-s)}) + (P_{Diode} \times R_{th(j-c)}) \tag{13}$$

where T_S is the heat sink temperature and P_T is the total power loss of the IGBT module. The case to sink $R_{th(c-s)}$ and junction to case $R_{th(j-c)}$ thermal resistances can

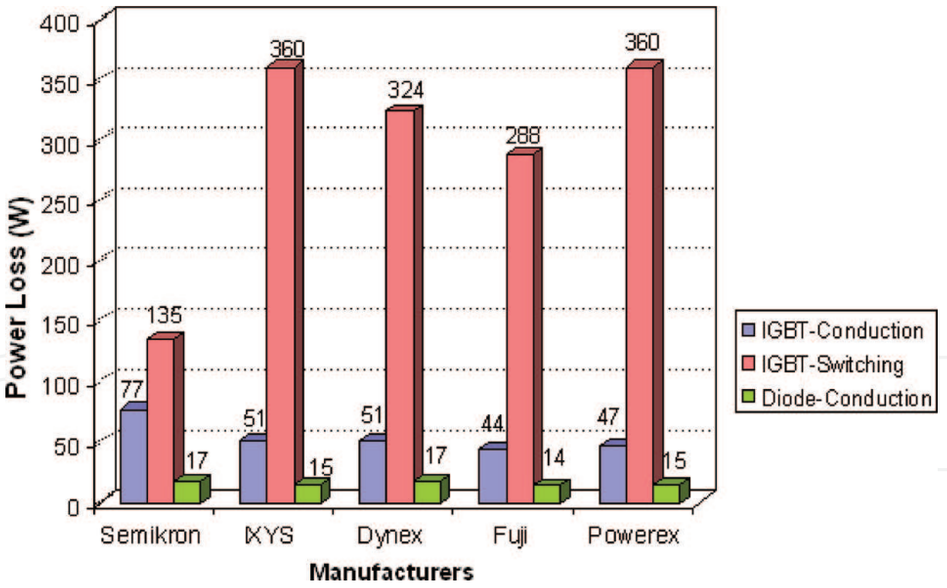

Figure 3.
HV-side IGBT and anti-parallel diode power loss comparison for various manufacturers.

be obtained from the device datasheet. The total power losses of the IGBTs and the antiparallel diode of the HV side of the DAB converter are compared for devices with ratings similar to 1200 V, 300 A from five different manufacturers:

- SKM300GB125D from Semikron, which has a rating of 1200 V, 300 A at T_{case} = 25°C;
- MII300-12A4 from IXYS, which has a rating of 1200 V, 330 A at T_{case} = 25°C;
- DIM200WHS12-A000 from Dynex Semiconductor, which has a rating of 1200 V, 200 A at T_{case} = 80°C;
- 2MB1300U4H-120 from Fuji Semiconductor, which has a rating of 1200 V, 400 A at T_{case} = 25°C; and
- CM300DY-24A from Powerex, which has a rating of 1200 V, 300 A at T_{case} = 25°C.

The power losses of IGBTs and anti-parallel diodes are predicted for the worst-case operating condition and are depicted in **Figure 3**. Based on a comparison of the losses of all devices, the ultra-fast SKM300GB125D 1200 V, 300 A phase leg IGBT modules from Semikron [28] are selected for the HV side of the converter due to their low loss. As shown in **Figure 3**, the switching power losses of the IGBTs are significant and are a major contributor to the overall power loss due to the high switching frequency and high turn-off current.

3. Power loss estimation of LV-side devices of the DAB DC-DC converter

The power loss of LV-side devices is predicted using a procedure similar to that discussed in Section 2. The main difference is that the shape of the LV-side device currents differs from those of the HV-side devices due to the phase shift introduced between the HV- and LV-side bridges as shown in **Figure 2**. The transistor and diode current equations during the on-state are

$$I_T = \frac{\frac{1}{2} \times I_{L1} \times \left(\frac{dT_S}{2} - t_B\right)}{\left(\frac{dT_S}{2} - t_B\right)} \quad (14)$$

and

$$I_D = \frac{\frac{1}{2} \times (I_P \times t_B) + \frac{1}{2} \times (I_{L1} + I_P) \times \left(\frac{T_S}{2} - \frac{dT_S}{2}\right)}{\left(\frac{T_S}{2} - \frac{dT_S}{2} + t_B\right)} \quad (15)$$

Similar to the HV side, the on-state and switching power losses of the IGBTs and the antiparallel diode of the LV side of the DAB converter are compared for devices with ratings similar to 600 V, 700 A at T_{case} = 25°C from four leading manufacturers:

- SKM600GB066D from Semikron, which has a rating of 600 V, 760 A;
- CM600DY-12NF from Mitsubishi, which has a rating of 600 V, 600 A;
- 2MB1600U2E-060 from Fuji Semiconductor, which as a rating of 650 V, 600 A; and
- CM600DY-12NF from Powerex, which has a rating of 600 V, 600 A.

Figure 4 portrays the power loss comparison of an LV IGBT and antiparallel diode for each module. As shown in **Figure 4**, all IGBT modules exhibit similar performance. During the forward conduction mode (charging mode), the diodes perform the rectification function. Hence, the conduction losses of the diodes are predominant. When the power flow reverses, the loss values are exchanged between the diode and IGBT. The phase leg modules from Semikron have lower losses than the other devices. In addition, the Semikron module has a maximum junction temperature of 175°C, whereas the other modules have a maximum junction temperature of 150°C. Hence, the Semikron SKM600GB066D high-temperature phase leg IGBT modules [29], which have a rating of 600 V, 760 A, were chosen for the LV side of the converter.

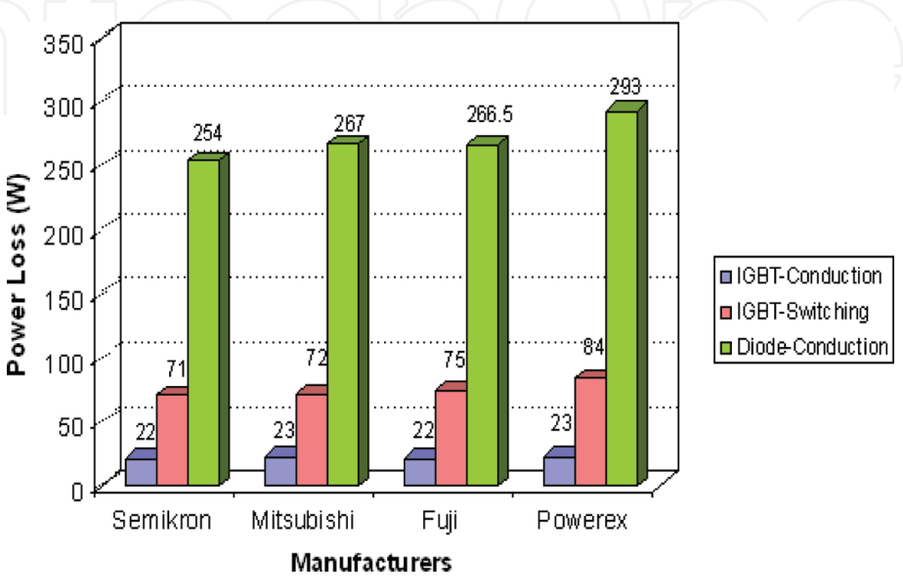

Figure 4.
LV-side IGBT and antiparallel diode power loss comparison from various manufacturers.

4. Experimental results

Experiments were performed for the HV- and LV-side devices of the converter using a suitable reactive load. A 39 μH air-core inductor was used for HV bridge testing by phase shifting the two half-bridge legs of the IGBTs, and the devices are subjected to maximum currents. Because the load was purely reactive, the current drawn from the source was used to meet the device conduction losses, switching losses, and the losses due to the passive components. A photograph of the DAB converter prototype is shown in **Figure 5**. Experimental results are shown in **Figures 6** and 7 for the HV-side IGBTs of the DAB converter for 540 V, 80 A operation with and without the snubber capacitor.

A 47 nF snubber capacitor was used on the HV side to minimize the turn-off losses and improve the switching transient of the HV-side IGBTs. A direct mount snubber capacitor type was used with a reduced effective series resistance (ESR) and with a low effective series inductance (ESL). As evident from the waveforms shown in **Figures 6** and 7, the diode begins conduction before the transistor, which ensures ZVS turn-on at peak current and ZVS/ZCS during turn-off. Similarly, the IGBT has ZVS/ZCS turn-on and ZVS turn-off at peak current.

The power loss measured during the experiments for the HV bridge converter at 16.6 kVA operation is plotted in **Figure 8**. Two cases are considered: in the first, a 47 nF

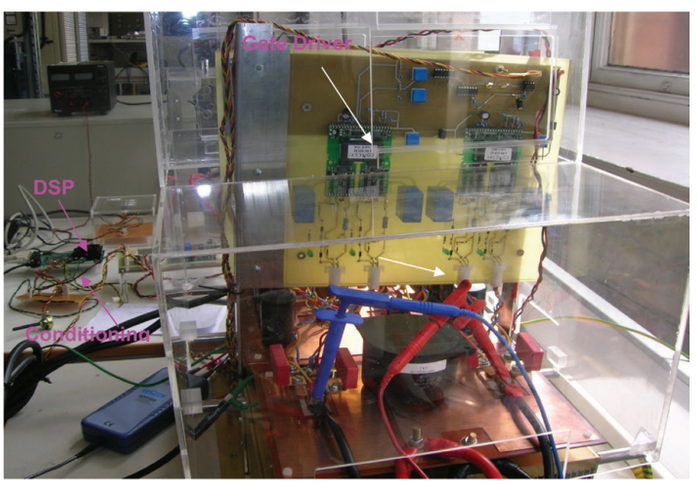

(a)

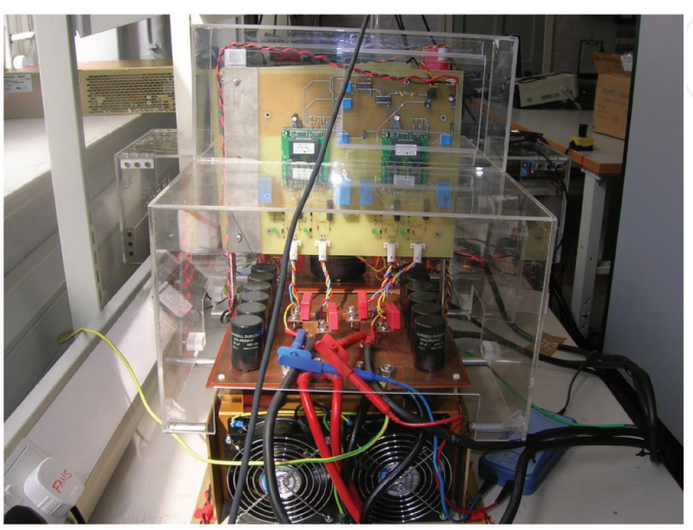

(b)

Figure 5.
Photographs of the DAB converter prototype: (a) front view and (b) back view.

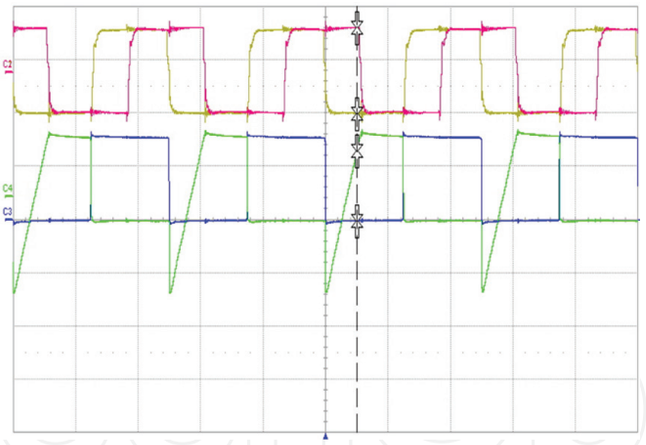

Figure 6.
Experimental results for the HV-side converter. V_{in} = 540 V, L = 39 μH, V_{Lrms} = 363 V, I_{Lrms} = 65.6 A, f_s = 20 kHz, I_{OFF} = 80 A. Channel 1 (yellow)—gate pulse of transistor A_2, 10 V/div. Channel 2 (pink)—gate pulse of transistor B_2, 10 V/div. Channel 3 (blue)—IGBT A_1 voltage, 350 V/div. Channel 4 (green)—IGBT A_1 current, 50A/div. Time scale: 20 μs/div.

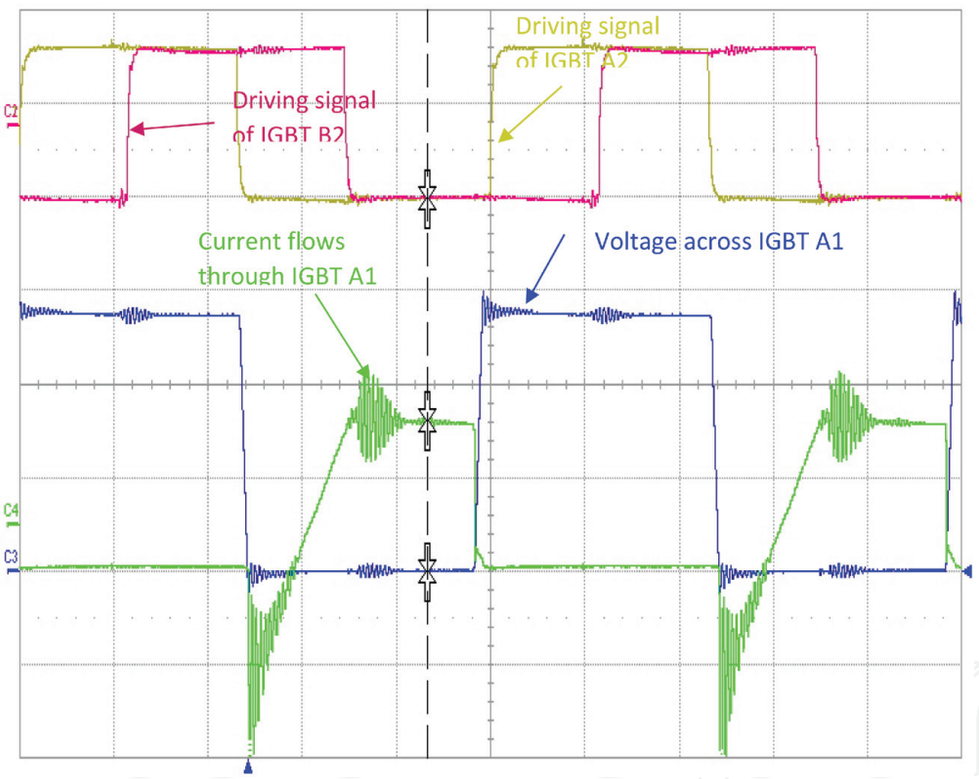

Figure 7.
Experimental results for the HV-side converter with a 47 nF snubber. V_{in} = 540 V, I_{in} = 1.318 A, L = 39 μH, f_s = 20 kHz, V_{Lrms} = 363 V, I_{Lrms} = 65.6 A, I_{OFF} = 80 A, R_G = 3 Ω, C_s = 47 nF. Time scale: 10 μs/div. Channel 1 (yellow)—gate pulse of transistor A2, 10 V/div. Channel 2 (pink)—gate pulse of transistor B2, 10 V/div. Channel 3 (blue)—IGBT A1 voltage, 200 V/div. Channel 4 (green)—IGBT A1 current, 50A/div.

snubber capacitor is connected across each of the four IGBTs of the HV-side bridge; in the second, no snubber capacitor is used. The power losses of the leading-phase and lagging-phase leg devices are displayed separately in **Figure 8** due to different conduction intervals of the devices. Power losses in the cables, busbar, and connections are neglected. Due to the ZCS turn-off of the diodes, their reverse recovery losses are neglected; due to ZVS/ZCS turn-on of the IGBTs, their turn-on losses are omitted. As shown in **Figure 8**, the air-core inductor copper losses are high although it has only 11 turns. Diode and IGBT conduction losses, however, remain approximately constant with or without the snubber capacitors. As evident in **Figure 8**, there is a considerable reduction in turn-off losses when the snubber capacitor is used.

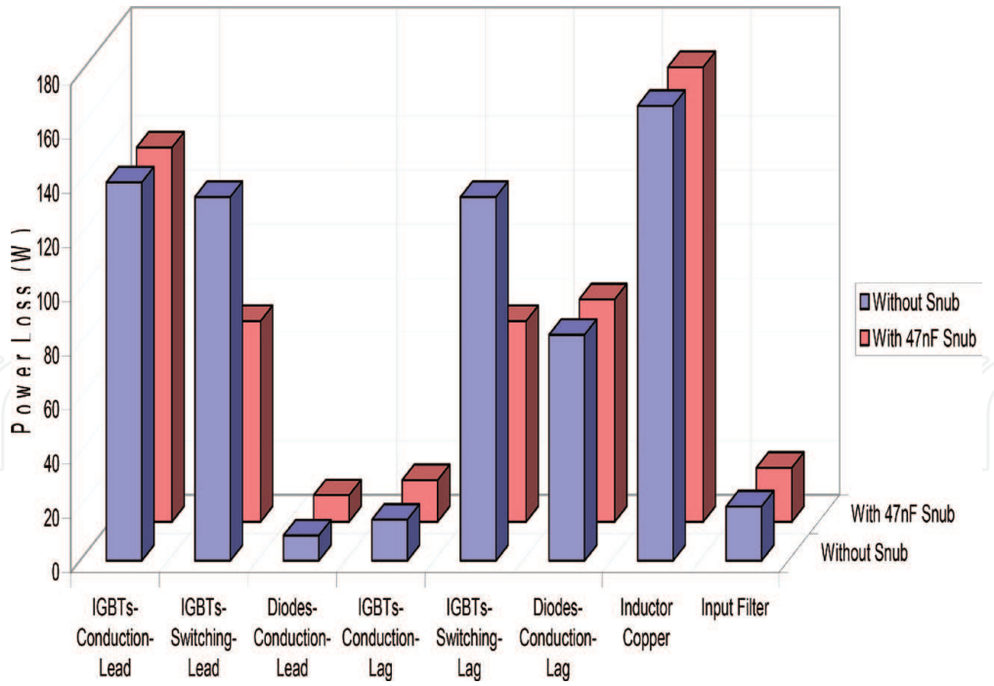

Figure 8.
Experimental power loss breakdown of the HV-side converter with and without the snubber capacitor. V_{in} = 540 V, L = 39 μH, f_s = 20 kHz, I_{OFF} = 80 A, V_{Lrms} = 363 V, I_{Lrms} = 65.6 A, R_G = 3 Ω.

The LV-side devices of the converter were tested, and the LV-side IGBTs were subjected to a peak current of 300 A at 125 V. The two legs of the LV-side bridge were connected through an air core inductor with a value of 4.17 μH. An external electrolytic capacitor bank of 19.8 mF capacitance (comprising three 6.6 mF capacitor banks) was added to the DC supply to smooth the input ripple current. **Figure 9** shows the current and voltage waveforms of the leading-leg IGBT and the driving signals of the IGBTs, D_2 and C_2. A CWT15 Rogowski current probe with a sensitivity of 2 mV/A was used

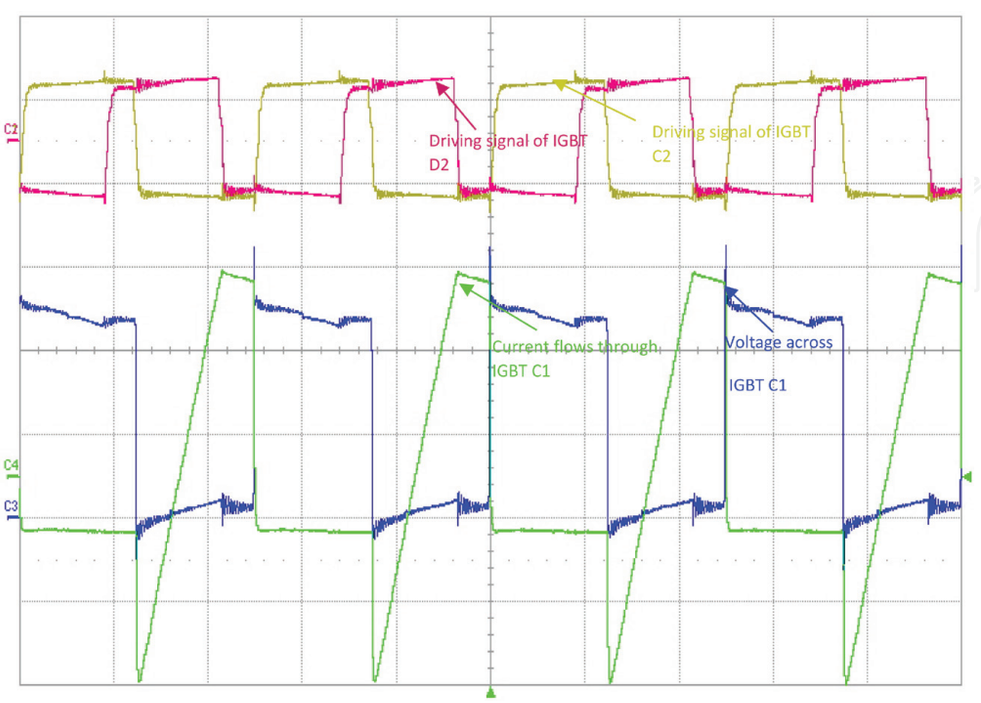

Figure 9.
Experimental results for the LV-side converter without the snubber. V_{in} = 125 V, I_{in} = 10.51 A, L = 4.17 μH, V_{Lrms} = 106 V, I_{Lrms} = 202 A, f_s = 20 kHz, I_{OFF} = 300 A, R_G = 2.5 Ω. Time scale: 20 μs/div. Channel 1 (yellow)—gate pulse of transistor C2, 10 V/div. Channel 2 (pink)—gate pulse of transistor D2, 10 V/div. Channel 3 (blue)—IGBT C1 voltage, 100 V/div. Channel 4 (green)—IGBT C1 current, 100A/div.

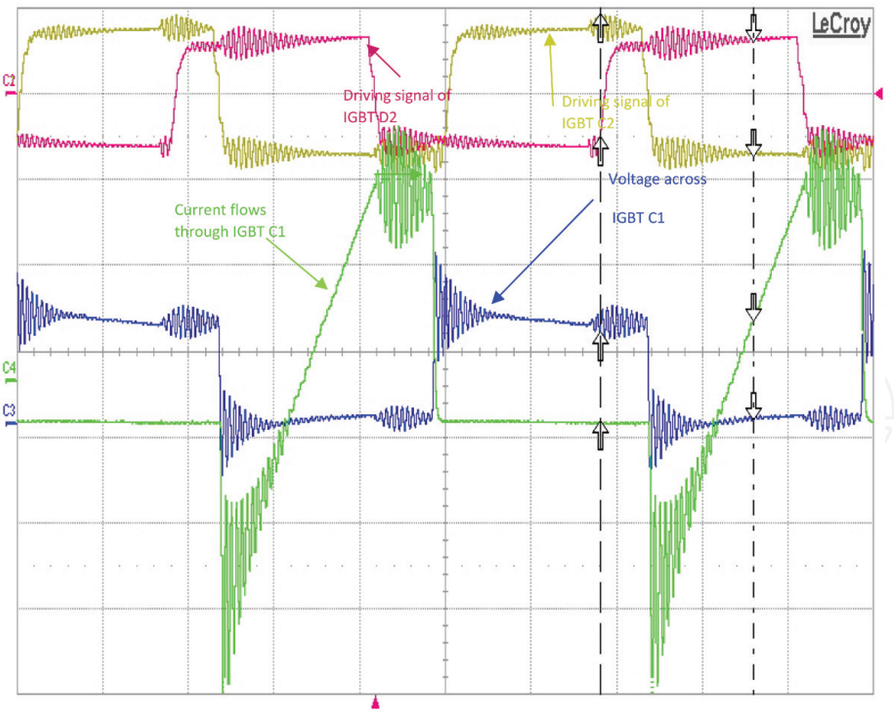

Figure 10.
Experimental waveforms of the LV-side converter with a 100 nF snubber. V_{in} = 125 V, I_{in} = 9.29 A, L = 4.17 μH, V_{Lrms} = 106 V, I_{Lrms} = 202 A, f_s = 20 kHz, I_{OFF} = 300 A, R_G = 2.5 Ω. Time scale: 10 μs/div. Channel 1 (yellow)—gate pulse of transistor C2, 10 V/div. Channel 2 (pink)—gate pulse of transistor D2, 10 V/div. Channel 3 (blue)—IGBT C1 voltage, 100 V/div. Channel 4 (green)—IGBT C1 current, 100A/div.

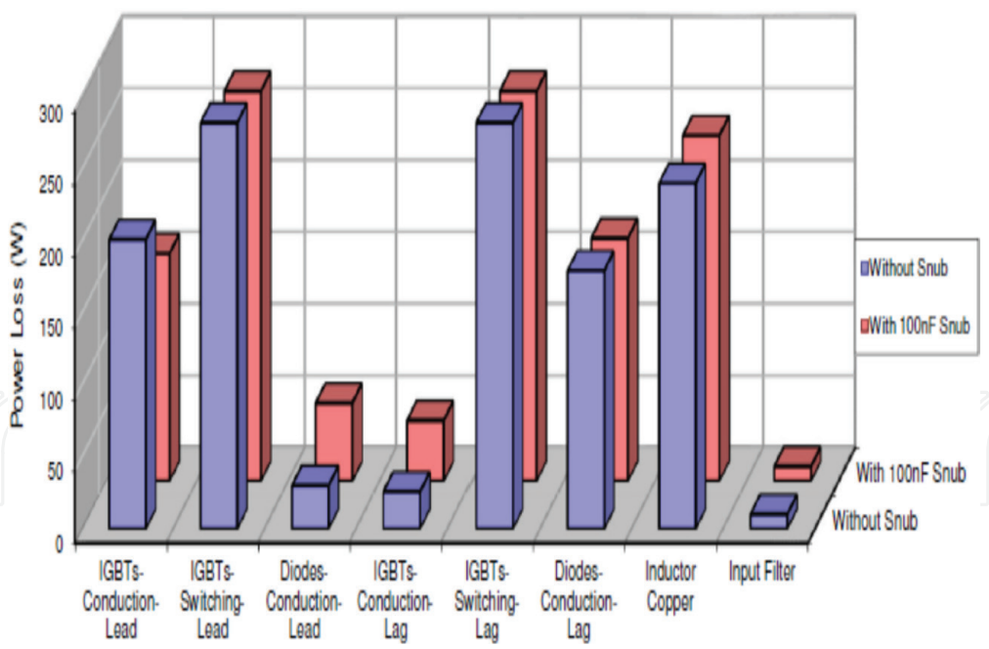

Figure 11.
Experimental measurement of power loss on the LV-side converter with and without the snubber. V_{in} = 125 V, L = 4.17 μH, f_s = 20 kHz, I_{OFF} = 300 A, V_{Lrms} = 106 V, I_{Lrms} = 202 A, R_G = 2.5 Ω.

to measure the device currents. The measured current fall-time is 205 ns for the initial current fall time and 620 ns for the tail current fall duration. High-frequency ringing is observed in the device waveforms when the snubbers are introduced across the devices. This may be resonance due to parasitic inductances of the module (with values of 15–20 nH), the busbars, and the snubber capacitor connections.

The input power drawn from the source using 100 nF snubber capacitors is lower than those observed for other snubbers. Moreover, a significant reduction

in *dv/dt* during the switching transients is observed. Hence, 100 nF snubbers are chosen for the LV-side IGBTs. **Figure 10** shows the experimental waveforms for the LV-side IGBT C_1 with a 100 nF snubber capacitor. **Figure 11** illustrates the power loss breakdown for the LV-side bridge converter at 19.2 kVA operation with and without the snubber capacitors, as determined from the measurements. The IGBT switching losses are dominant. Power losses due to cables, busbars, and connections are not included. When 100 nF snubber capacitors are connected across the IGBTs, no significant reduction in switching losses occurs. The experimental power loss using the 100 nF snubber is 135 W, and *dv/dt* during the switching transient is reduced significantly, thereby minimizing the device stresses.

Comparisons of the theoretical and practical power losses of the HV- and LV-side devices are shown in **Figures 12** and **13**, respectively, for the leading leg devices to validate the mathematical models describing the device current equations. A close correlation between the calculated and experimental power loss values is observed, which demonstrates the effectiveness of the mathematical models presented.

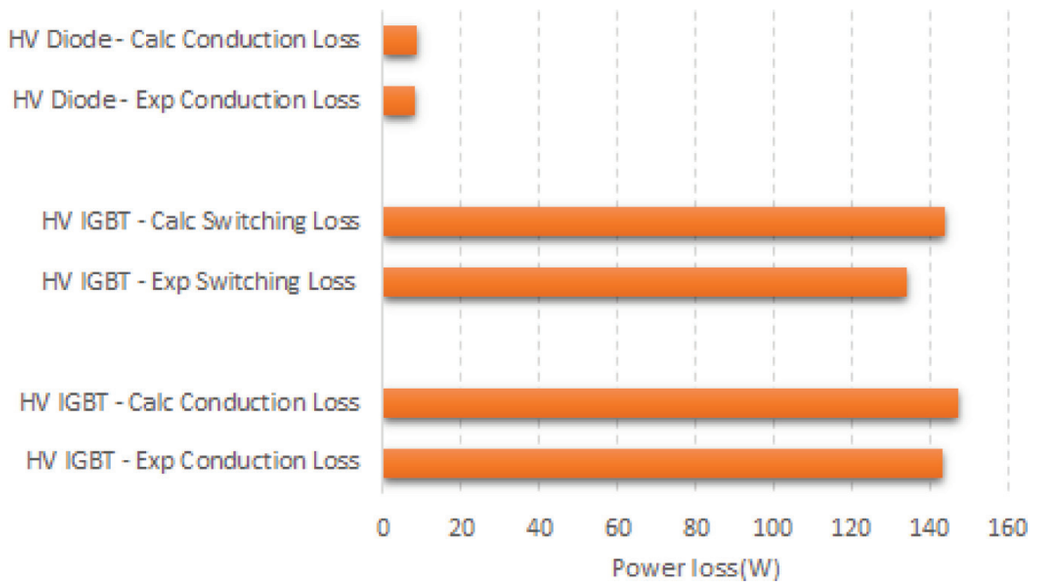

Figure 12.
Power loss comparison of HV-side devices—calculated (Calc) and experimental (Exp).

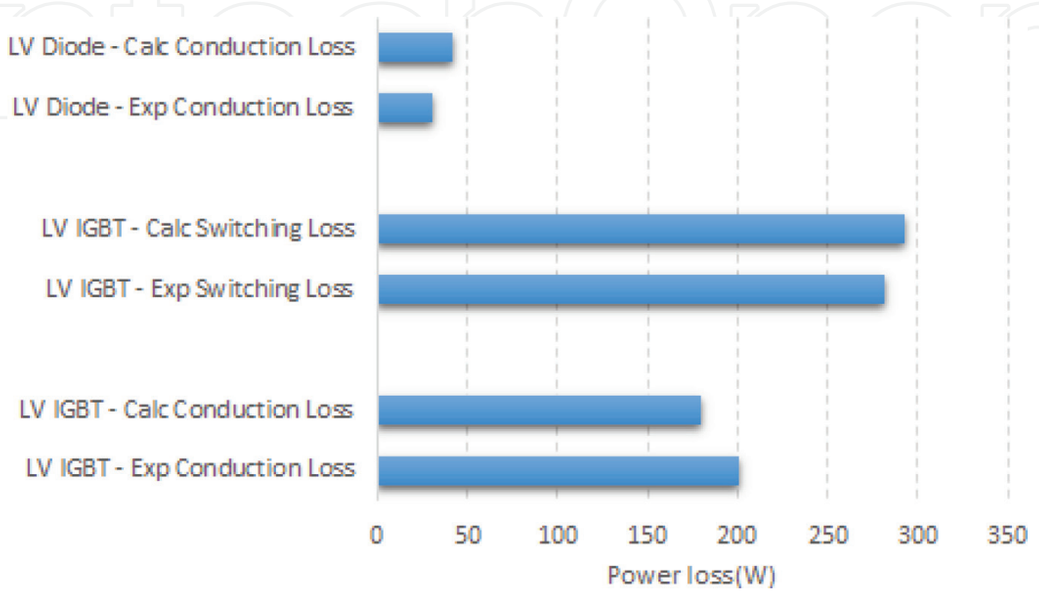

Figure 13.
Power loss comparison of LV-side devices—calculated (Calc) and experimental (Exp).

5. Conclusion

Power loss analysis of IGBTs in a high-voltage high-power DAB DC-DC converter intended for use in an aerospace energy storage system was presented. The guidelines for selecting the appropriate IGBTs for a 20 kW, 540/125 V, 20 kHz DAB DC-DC converter prototype suitable for aerospace applications were given. The important parameters provided in the device datasheet for calculating the device power losses were discussed. Power loss analysis was performed for HV IGBTs corresponding to five leading manufacturers and LV IGBTs corresponding to four leading manufacturers based on the DAB converter prototype design. Apart from the guidelines given in this chapter, some IGBT manufacturers offer customer support for device loss estimation through a software package. Such software packages may be used for preliminary studies to estimate the device losses and the junction temperature for various operating conditions. In this work, experimental results were presented for 540 V, 80 A peak current operation on the HV-side IGBT, and 125 V, 300 A peak current on the LV-side IGBT. Using snubber capacitors on the HV side of the converter resulted in a nearly 45% reduction of IGBT switching losses. Introducing snubber capacitors on the LV-side devices created parasitic ringing, with no significant reduction of switching power losses. However, snubbers on the LV side did reduce the device stresses by limiting dv/dt. The experimental results demonstrate that the use of snubber capacitors across IGBTs reduces switching losses and device stresses and thus improves converter performance.

Acknowledgements

The author thanks Rolls-Royce plc and the Engineering and Physical Sciences Research Council (EPSRC), UK, for the DHPA scholarship at the University of Manchester.

Author details

Thaiyal Naayagi Ramasamy
School of Electrical and Electronic Engineering, Newcastle University International Singapore, Singapore

*Address all correspondence to: naayagi.ramasamy@ncl.ac.uk

References

[1] DeDoncker RWRW, Divan DM, Kheraluwala MH. A three-phase soft-switched high-power-density dc/dc converter for high power applications. IEEE Transactions on Industry Applications. 1991;**27**(1):797-806. DOI: 10.1109/28.67533

[2] Kheraluwala MH, Gascoigne RW, Divan DM, Baumann ED. Performance characterization of a high-power dual active bridge dc-to dc converter. IEEE Transactions on Industry Applications. 1992;**28**(6):1294-1301. DOI: 10.1109/28.175280

[3] Segaran D, Holmes DG, McGrath BP. Comparative analysis of single and three-phase dual active bridge bidirectional dc-dc converters. In: Proc. Australian Universities Power Engineering Conference; 2008. pp. 1-6

[4] Tripathi AK, Mainali K, Patel DC, Kadavelugu A, Hazra S, Bhattacharya S, et al. Design considerations of a 15-kV SiC IGBT-based medium-voltage high-frequency isolated DC–DC converter. IEEE Transactions on Industry Applications. 2015;**51**(4):3284-3294. DOI: 10.1109/TIA.2015.2394294

[5] Kadavelugu A, Bhattacharya S, Ryu S-H, Brunt EV, Grider D, Agarwal A, Leslie S. Characterization of 15 kV SiC n-IGBT and its application considerations for high power converters. In: Proc. IEEE Energy Conversion Congress and Expo; 2013. pp. 2528-2535

[6] Kadavelugu A, Bhattacharya S. Design considerations and development of gate driver for 15 kV SiC IGBT. In: Proc. IEEE Applied Power Electronics Conference and Expo; 2014. pp. 1494-1501

[7] Hazra S, Madhusoodhanan S, Bhattacharya S, Moghaddam GK, Hatua K. Design considerations and performance evaluation of 1200 V, 100 a SiC MOSFET based converter for high power density application. In: Proc. IEEE Energy Conversion Congress and Expo; 2013. pp. 4278-4285

[8] Wen H, Xiao W, Bin S. Non active power loss minimization in a bidirectional isolated DC–DC converter for distributed power systems. IEEE Transactions on Industry Applications. 2014;**61**(12):6822-6831. DOI: 10.1109/TIE.2014.2316229

[9] Oggier GG, Garcia GO, Oliva AR. Switching control strategy to minimize dual active bridge converter losses. IEEE Transactions on Power Electronics. 2009;**24**(7):1826-1838. DOI: 10.1109/TPEL.2009.2020902

[10] Wang Y, de Haan SWH, Ferreira JA. Potential of improving PWM converter power density with advanced components. In: Proc. 13th European Conference on Power Electronics and Applications; 2009. pp. 1-10

[11] Gao Y, Huang AQ, Krishnaswami S, Richmond J, Agarwal AK. Comparison of Static and Switching Characteristics of 1200 V 4H-SiC BJT and 1200 V Si-IGBT. IEEE Transactions on Industry Applications. 2008;**44**(3):887-893. DOI: 10.1109/TIA.2008.921408

[12] Nomura T, Masuda M, Ikeda N, Yoshida S. Switching characteristics of GaN HFETs in a half bridge package for high temperature applications. IEEE Transactions on Power Electronics. 2008;**23**(2):692-697. DOI: 10.1109/TPEL.2007.915671

[13] Semikron. Operation Principle of Power Semiconductors-Application Manual; 2008

[14] Semikron. Calculation of the Junction Temperature-Hints for Application-3.2.22008. p. 146

[15] Fuji Electric. Fuji IGBT Modules Application Manual; 2004

[16] Naayagi RT. Selection of power semiconductor devices for the DAB DC-DC converter for aerospace applications. In: Proc. IEEE 11th International Conference on Power Electronics and Drive Systems; 2015. pp. 499-502

[17] Advanced Power Technology. IGBT Tutorial Application Note APT0201. Rev. B. 2002

[18] Microsemi. Advanced IGBT Driver Application Manual-Application Note 1903; 2006

[19] Powerex. General Considerations for IGBT and Intelligent Power Modules-Application Note A10; 2008

[20] International Rectifier. Application Characterization of IGBTs-Application Note AN-990, rev.2; 2008

[21] IXYS. Choosing the Appropriate Component from Data Sheet Ratings and Characteristics-Technical information IXAN0056; 2008

[22] Ramasamy TN. Bidirectional DC-DC converter for aircraft electric energy storage systems [PhD thesis]. School of Electrical and Electronic Engineering, University of Manchester; 2010

[23] International Rectifier. IGBT or MOSFET: Choose Wisely-Application note; 2008

[24] Semikron. Power Modules: Special Features of Multi-Chip Structures-Application Note-1.4, AN1404; 2014

[25] Semikron. New Low-Inductive IGBT Module Constructions for High Currents and Voltages-Application Note-1.5.4; 2014

[26] Semikron. New Developments in MOSFET and IGBT Technology-Application Note-1.2.4;2014

[27] Naayagi RT, Forsyth AJ, Shuttleworth R. High-power bidirectional DC-DC converter for aerospace applications. IEEE Transactions on Power Electronics. 2012;**27**(11):4366-4379. DOI: 10.1109/TPEL.2012.2184771

[28] Semikron. Ultrafast IGBT Module SKM300GB125D Datasheet; 2009

[29] Semikron. Trench IGBT Module SKM600GB066D Datasheet; 2009